applied sciences

Article

A Convolutional Neural Network-Based Corrosion Damage Determination Method for Localized Random Pitting Steel Columns

Xu Jiang [1], Hao Qi [1], Xuhong Qiang [1,*], Bosen Zhao [2] and Hao Dong [3]

[1] College of Civil Engineering, Tongji University, Shanghai 200092, China; jiangxu@tongji.edu.cn (X.J.); 2232326@tongji.edu.cn (H.Q.)
[2] Shanghai Research Institute of Building Sciences Co., Ltd., Shanghai 200032, China
[3] China Design Group Co., Ltd., Nanjing 210014, China
* Correspondence: qiangxuhong@tongji.edu.cn

Abstract: As one of the most common forms of corrosion in the marine environment, pitting corrosion can have a detrimental impact on the ultimate strength of steel columns. Pitting pits are usually covered by corrosion products, and the detection of pitting is very difficult, so how to effectively identify random pitting corrosion on steel columns has become a very vital issue. In this paper, a deep-learning-based pitting damage determination method for steel columns is investigated by combining numerical simulation and theoretical analysis, which was validated by experimental results. First, a multi-parameter localized pitting corrosion model was proposed that considered the pitting corrosion randomness in time and space distribution. Second, the relationship between the ultimate strength and corrosion rate of steel columns was analyzed. Finally, a steel column damage determination framework was constructed based on the convolutional neural network. Results showed that the ultimate strength and corrosion rate developed different trends in various corrosion regions, and a damage determination accuracy of 90.2% could be achieved by the neural network after training, which satisfied the practical engineering requirements. This study lays the groundwork for further application of deep learning to the research on the pitting damage to steel structures.

Keywords: pitting corrosion; corrosion damage determination; deep learning; CNN; steel column

Citation: Jiang, X.; Qi, H.; Qiang, X.; Zhao, B.; Dong, H. A Convolutional Neural Network-Based Corrosion Damage Determination Method for Localized Random Pitting Steel Columns. *Appl. Sci.* **2023**, *13*, 8883. https://doi.org/10.3390/app13158883

Academic Editor: José António Correia

Received: 14 July 2023
Revised: 28 July 2023
Accepted: 31 July 2023
Published: 1 August 2023

1. Introduction

Metal corrosion, which is a chemical or electrochemical reaction between materials and severe environments [1], directly leads to the deterioration of material properties [2] and reduces the load-bearing capacity of infrastructures [3]. According to the World Corrosion Organization, the annual cost of corrosion repair is USD 2.5 trillion, accounting for 3% of the global GDP [4]. The high humidity and salinity in the marine environment make materials easily susceptible to corrosion [5]. As the most prevalent type of corrosion [6] in the marine environment, pitting is one of the most destructive forms of corrosion of steel structures [7].

Research on pitting is generally divided into experimental study and numerical simulation [8–10]. Since pitting experiments require many experimental resources and the relevant test parameters are difficult to control, numerical simulation has become a more common method, and the pitting modeling is crucial to the accuracy of numerical simulation. Jiang et al. [11,12] investigated the effect of corrosion pits on the ultimate strength-carrying capacity of mild steel rectangular plates under uniaxial compression. Comparison between the finite element simulation results and the equations showed a satisfactory fit. Nakai et al. [13] conducted a series of tensile tests to investigate the effect of pitting on the tensile strength of members and found that the tensile strength decreases as the thickness loss from pitting increases, and that the decrease in the tensile strength of members due to pitting is greater than the decrease in the tensile strength of members due to uniform thickness loss. Studying pitting modeling is important for an in-depth understanding of the mechanism of the pitting action and for the corresponding preventive detections. Pidaparti et al. [14] used a three-dimensional metacellular automaton model to completely simulate the process of localized etching pits on metal surfaces with time, but their model is too complex to be used in practice. To use pitting models for the study of large-scale samples, batch pitting modeling is needed directly from the perspective of pitting parameters. The common pitting parameters include the shape, distribution, and geometry of pitting. Research on the pitting corrosion on suspension wires found that the pits in the corroded wires had four typical shapes, and the maximum pitting depth fitted a Weibull distribution while the length and the width fitted a lognormal distribution [15]. Sharifi et al. [16] used a finite element model with a uniform arrangement of pitting pits to investigate the load-carrying capacity of the members after pitting. Zhang [17] proposed a mathematical model to qualify the extreme value of pitting corrosion depth according to aging time. Regarding the depth distribution of pitting pits, Ossai et al. [18] successfully predicted the depth distribution of pitting pits in oil and gas pipelines by developing a Markov model with an accuracy of more than 90%; Rivas [19] collected corrosion data by immersion tests and found that the depth of pitting pits had a bimodal Gaussian distribution; Melchers [20] found that the Weibull distribution could better describe the depth distribution of pitting pits on carbon steel surfaces. Uniform and random distributions are two methods commonly used to express the distribution of pitting pit locations. The uniform distribution simplifies the modeling process but it neglects the randomness of pitting, so the random distribution has better accuracy, comparably [21]. Within the existing research, there are few studies related to the random distribution of pitting components, which is a significant drawback to a better understanding of the pitting mechanism.

Considering the hazards of pitting damage, the lack of a timely determination of pitting damage will greatly harm economic prospects and resources, which is not in accordance with the Sustainable Development Goal [22]. Cawley et al. [23] were the first to propose a damage identification method using intrinsic frequency. Salawu et al. [24] presented various methods of intrinsic frequency damage detection and pointed out that since the stress is minimum at the point where the modal displacement is zero, the site of damage is in the vicinity of the point where this modal displacement is zero. However, the intrinsic frequency is less sensitive to pitting damage and cannot be accurately determined [25,26]. Pandey et al. [27] developed a damage identification method based on the vibration mode and found that the vibration mode change occurred at the damaged area, which was positively correlated with the damage degree. Wang et al. [28] developed a new method for damage localization and severity estimation based on the application of modal strain energy. This method requires information on the variation of only a few lower intrinsic frequencies to locate the damage and estimate its severity. Related studies have shown that the vibration mode has a good mapping for corrosion damage identification [29,30], which can be used in pitting corrosion determination. According to the current literature, there are still large gaps in the relevant research.

Machine learning, as an efficient analytical tool with proven powerful learning and nonlinear fitting capabilities, has played an important role in the research on the pitting corrosion of steel components in recent years. Six machine learning models with eight different combinations of input variables were assessed using eleven statistic indicators to predict the maximum pitting corrosion depth in oil and gas pipelines [31]; as a result, the Kriging model had the best performance and accuracy. Ossai [32] proposed a Gradient Boosting Machine with Principal Component Analysis to predict the corrosion defect depth growth of oil pipelines with high accuracy. The author utilized the parameters of the pipelines to predict the corrosion conditions in the future using the proposed Principal Component Analysis and Gradient Boosting Machine (PCA-GBM) method. Deep learning, as a further development, has taken pitting research to a new level. A deep-learning framework was developed to find the contributions of alloying elements to local pitting resistance, which benefited the investigation of corrosion-resistant alloys for alloy design [33]. Researchers have conducted many studies related to pitting using deep learning. Sharifi et al. [34] used the artificial neural network (ANN) method to estimate the load-carrying capacity of deteriorated steel beam models with different levels of pitting under patch loading. Ossai [35] developed a subspace-clustered neural network model to search for the relationship between pipeline corrosion and related input parameters using particle swarm optimization in a feed-forward network. Barai [36] et al. used truss bridge node displacements as a damage indicator and also used ANNs to predict the damage to truss bridge unit stiffness, still based on a finite element model, with no foot-size test to confirm the practicability of the method. As for the stress–strain properties of pitting steel components, related studies found that the yield platform of the load–displacement curve disappeared when pitting corrosion occurred in steel components, and ultimate strength, yield strength, as well as elongation were correlated with the pitting conditions [37]. The convolutional neural network (CNN) is a kind of matrix feature extraction using convolutional kernels that has a powerful learning ability. The Faster R-CNN technique has already been used for computer visual inspection of the steel corrosion and bolt corrosion and determined them to be 91.8% and 86.1% AP, respectively [38]. Chun et al. [39] used a deep-learning method to calculate the effective thickness of the shell models to equivalently substitute the solid models, which were utilized to evaluate the tensile performance of the pitting components. Based on previous research, the combination of deep learning and pitting damage determination will greatly stimulate pitting damage research and is of high practical value.

This paper proposes a pitting damage determination method based on the convolutional neural network for steel column components, which uses convolutional neural networks to determine the degree of pitting damage to steel columns by extracting the vibration characteristics of the members. First, a multi-parameter localized random pitting model is proposed to describe random pitting in combination with time-varying features and spatial distribution. Then, the mechanical properties of the pitting steel column members are analyzed, and the relationship between the ultimate strength of the specimens and the corrosion rate is investigated. Finally, a convolutional neural network framework based on component vibration modes is developed. The critical corrosion rate is used as the criterion for component damage determination training; in addition, the effectiveness and accuracy of the network are analyzed.

2. Pitting Model

Cylindrical pits were employed herein to simulate pitting corrosion. As a common form of corrosion in the marine environment, pitting has four dimensions: randomness in depth, size, location, and quantity. Conducting massive random pitting tests is resource-intensive. Therefore, it was necessary to establish a reasonable random pitting numerical model for the pitting determination of steel structures. This paper proposes a random pitting model framework based on pitting corrosion statistics and existing research results. Random pitting data were generated through Python, and finite element (FE) models corresponding to respective pitting data were established in FE software ABAQUS.

2.1. Multi-Parameter Localized Random Pitting Model

2.1.1. Depth and Size

The depth distribution of pitting pits conforms to the Weibull distribution [40,41]. The probability density function can be described as Equation (1), where α is the shape parameter, β is the scale parameter, and h is the depth of the pits. The probability distribution function Equation (2) can be obtained through the integration of Equation (1). Ren et al. [42] determined α and β as 1.432 and 2.319, respectively, by statistical calculation. Then Equation (1) can be described as Equation (3). The depth of a single pitting pit can be confirmed by a randomly generated probability in the range of [0,1]. Thus, the inverse function of the probability distribution function is required as Equation (4), where P is the probability of a certain value of h.

$$f_{(h)} = \begin{cases} \frac{\alpha}{\beta}\left(\frac{h}{\beta}\right)^{\alpha-1} & e^{-\left(\frac{h}{\beta}\right)^{\alpha}} & h \geq 0 \\ 0 & & h \leq 0 \end{cases} \tag{1}$$

$$F_{(h)} = \int_{-\infty}^{h} \left[\frac{\alpha}{\beta}\left(\frac{h}{\beta}\right)^{\alpha-1} e^{-\left(\frac{h}{\beta}\right)^{\alpha}}\right] dh = 1 - e^{-\left(\frac{h}{\beta}\right)^{\alpha}} h \geq 0 \tag{2}$$

$$F_{(h)} = 1 - e^{-\left(\frac{h}{1.432}\right)^{2.319}} h \geq 0 \tag{3}$$

$$h = 1.432[\ln(1-P)]^{\frac{1}{2.319}} \tag{4}$$

Wang et al. [43] investigated the relationship between the diameter–depth ratio and time and obtained the time-varying function of the diameter–depth ratio, which can be described as Equations (5)–(7), where λ is the diameter–depth ratio and t is the corrosion time. The tower limit of ultimate strength in a 95% confidence interval is taken as F_u, and the diameter of the K_{th} in the pit can be calculated by Equation (8), where D_k is the diameter of the K_{th} pitting pit.

$$\lambda_r(t) = 0, t \in [0,\ 7] \tag{5}$$

$$\lambda_r(t) = 8.16 + 115.15 \times \left[1 - e^{\left(-\frac{t-6.6}{7.27}\right)}\right]^{1.12} \times e^{\left(-\frac{t-6.6}{1.74}\right)}, t \in [7,\ 12] \tag{6}$$

$$\lambda_r(t) = \begin{cases} 8.34 + 1.92 \times e^{\left(-\frac{t-12.00}{2.59}\right)} & 65\%\ confidence \\ 8.34 + 4.00 \times e^{\left(-\frac{t-12.00}{2.20}\right)} & 80\%\ confidence\ ,\ t \in [12,\ \infty) \\ 8.34 + 5.04 \times e^{\left(-\frac{t-12.00}{2.07}\right)} & 95\%\ confidence \end{cases} \tag{7}$$

$$D_{\mathrm{k}} = \lambda_{\mathrm{r}}(t) \cdot h_{\mathrm{k}} \tag{8}$$

2.1.2. Location

An X52Q grade high-strength seamless steel pipe specimen tested by Qin [44] was employed herein to validate the numerical model. The specimen was uniformly divided into eight pitting regions along the length dimension. The geometry of the specimen is shown in Figure 1 and Table 1, where the slenderness ratio ζ, which means the ratio of the calculated length of the specimen to the radius of gyration of the specimen section, controls the length of the specimen. Only pitting corrosion in one region was investigated herein. According to the division of eight local pitting regions, when the pit was generated in each section, it was necessary to guarantee that pits did not exceed the boundary. Thus, the coordinates of pits are constrained by Equation (9), where (x_i, y_i, z_i) are the coordinates of the pits, D_i is the diameter of i_{th} pit, and n is the region number. Furthermore, pits cannot be stacked, which is constrained by Equation (10), where θ_i, θ_k is the angle under polar coordinates, $Dis_{i,k}$ is the distance between two pits, and $L_{i,k}$ is sum of the radius of two pits. The conversion of polar and rectangular coordinates can be calculated by Equation (11).

$$\begin{cases} -\frac{d}{2} \leq x_{\mathrm{i}} \leq \frac{d}{2} \\ y_{\mathrm{i}} = \pm\sqrt{(d/2)^2 - (x_{\mathrm{i}})^2} \\ (n-1) \cdot s + \frac{D_{\mathrm{i}}}{2} \leq z_{\mathrm{i}} \leq n \cdot s - \frac{D_{\mathrm{i}}}{2} \end{cases} \tag{9}$$

$$\begin{cases} \Delta\theta = |\theta_\mathrm{i} - \theta_\mathrm{k}| \\ Dis_\mathrm{i,k} = \sqrt{(\Delta\theta \cdot d)^2 + (z_\mathrm{i} - z_\mathrm{k})^2} \\ L_\mathrm{i,k} = \frac{D_\mathrm{i}+D_\mathrm{k}}{2} \\ \forall \mathrm{k} \neq i,\ Dis_0 \leq L_0 \end{cases} \quad (10)$$

$$\begin{cases} \theta_\mathrm{i} = \arctan\left(\frac{y_\mathrm{i}}{x_\mathrm{i}}\right) & x_\mathrm{i} \geq 0, y_\mathrm{i} \geq 0 \\ \theta_\mathrm{i} = 2\pi + \arctan\left(\frac{y_\mathrm{i}}{x_\mathrm{i}}\right) & x_\mathrm{i} \geq 0, y_\mathrm{i} < 0 \\ \theta_\mathrm{i} = \pi + \arctan\left(\frac{y_\mathrm{i}}{x_\mathrm{i}}\right) & x_\mathrm{i} < 0 \end{cases} \quad (11)$$

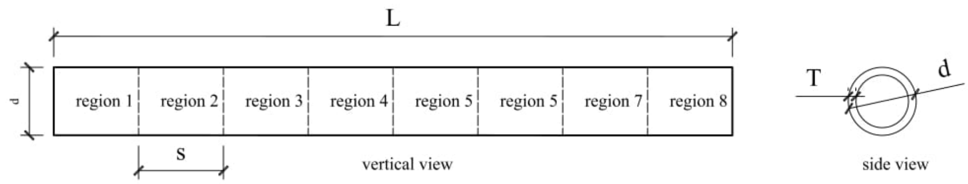

Figure 1. Schematic diagram of the specimen.

Table 1. Specimen geometry.

Slenderness Ratio ζ	Length L/mm	Thickness T/mm	Diameter d/mm	Section Length s/mm
20	1309	10	168.3	L/8
25	1636			
30	1964			
35	2291			

2.2. Finite Element Modeling

The pitting database was composed of different arrays of pit parameters. The data structure of the pitting database was $[k, ((x_i, y_i, z_i), d_i, h_i), ((x_{i+1}, y_{i+1}, z_{i+1}), d_{i+1}, h_{i+1})]$, where k is the region number. When proposing the database, specimen size, corrosion rate, and corrosion time were initially determined. Table 2 shows the initial parameters. What needs to be explained is P_0, which is defined as the volume ratio of pitting to its corrosion region. The geometry parameters were defined in Section 2.1. The corrosion rate P_0 and time t are ladder-value, which are shown in Table 3. Then λ can be calculated by Equations (6) and (7). N_0 is just an initial value of calculation that needs to be adjusted to obtain the number of the actual pits N_{act}. N_0 can be calculated by defining an initial corrosion depth h_0, multiplying it by the diameter-to-depth ratio λ to obtain an initial pit volume v_0, and finally calculating N_0 using the corrosion rate. The calculated method of N_0 is determined by Equation (12), where v is the volume of the specimen, and $h_0 = \frac{T}{2}$ is the assumed corrosion depth, which was determined after many attempts. Afterward, the depths h_i and diameter D_i of N_0 pits can be calculated by Equations (4) and (8), where P is randomly selected as N_0 times in (0,1). Figure 2 shows the adjustment from N_0 to N_{act}. Finally, the coordinates of N_{act} pits can be generated using the method in Section 2.1.2 and the corrosion database can be completed.

$$N_0 = \frac{4v}{n\pi(h_0\lambda)^2 h_0} \quad (12)$$

Table 2. Initial parameters of the specimen.

Parameter	Unit	Illustration
c	mm	Length of specimen
d	mm	Diameter of specimen
T	mm	Thickness
n	%	Number of regions
P_0	%	Corrosion rate
t	year	Corrosion time
N_0	-	Initial pit number

Table 3. Corrosion time t and rate P_0.

t	P_0
7 9 11	0.02,0.04,0.06,0.08
15 20 25 30 35 40	0.10,0.12,0.14,0.16,0.18

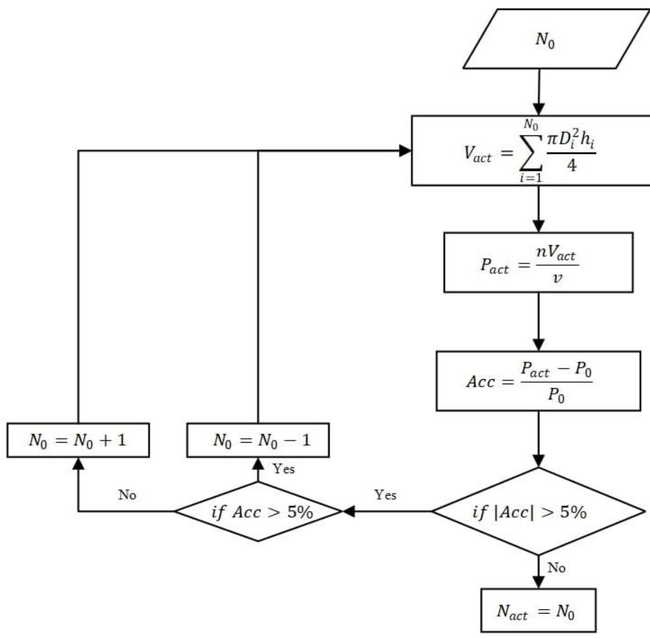

Figure 2. Adjustment operation from N_0 to N_{act}.

To assist the finite element analysis, a Python script was used to create a secondary development with ABAQUS finite element software, such as batching modeling, meshing, submitting, and outputting. The element type was C3D10, composed of 10 nodes, which is applicable for irregular solid geometric models. Boolean operations were executed when generating pits on specimen models. Figures 3 and 4 show the specimen's pitting model and mesh condition, respectively.

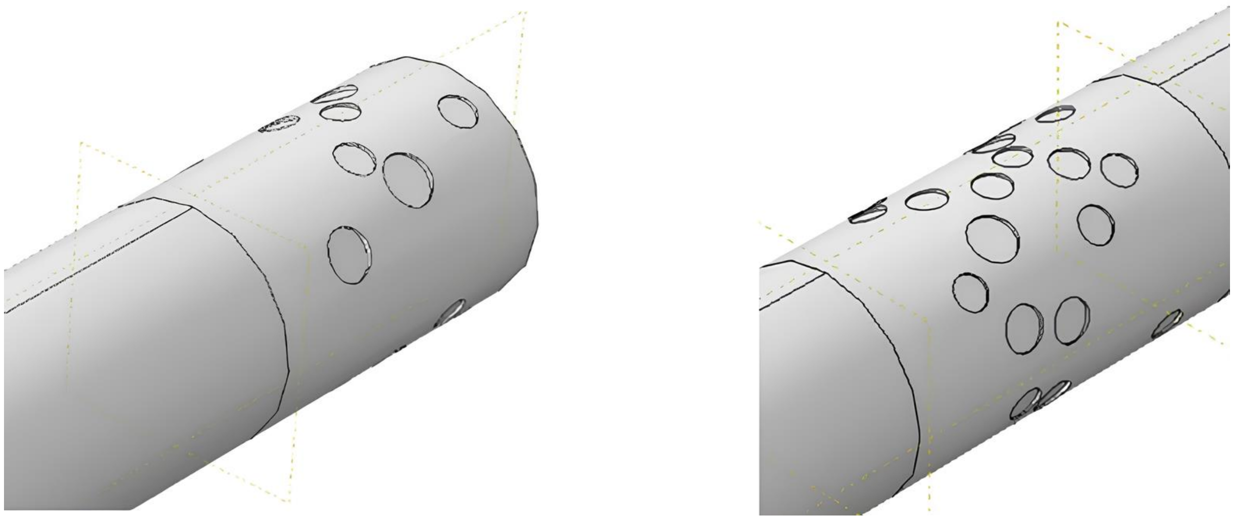
(a) (b)

Figure 3. Pitting FE model of the specimen. (**a**) End region; (**b**) central region.

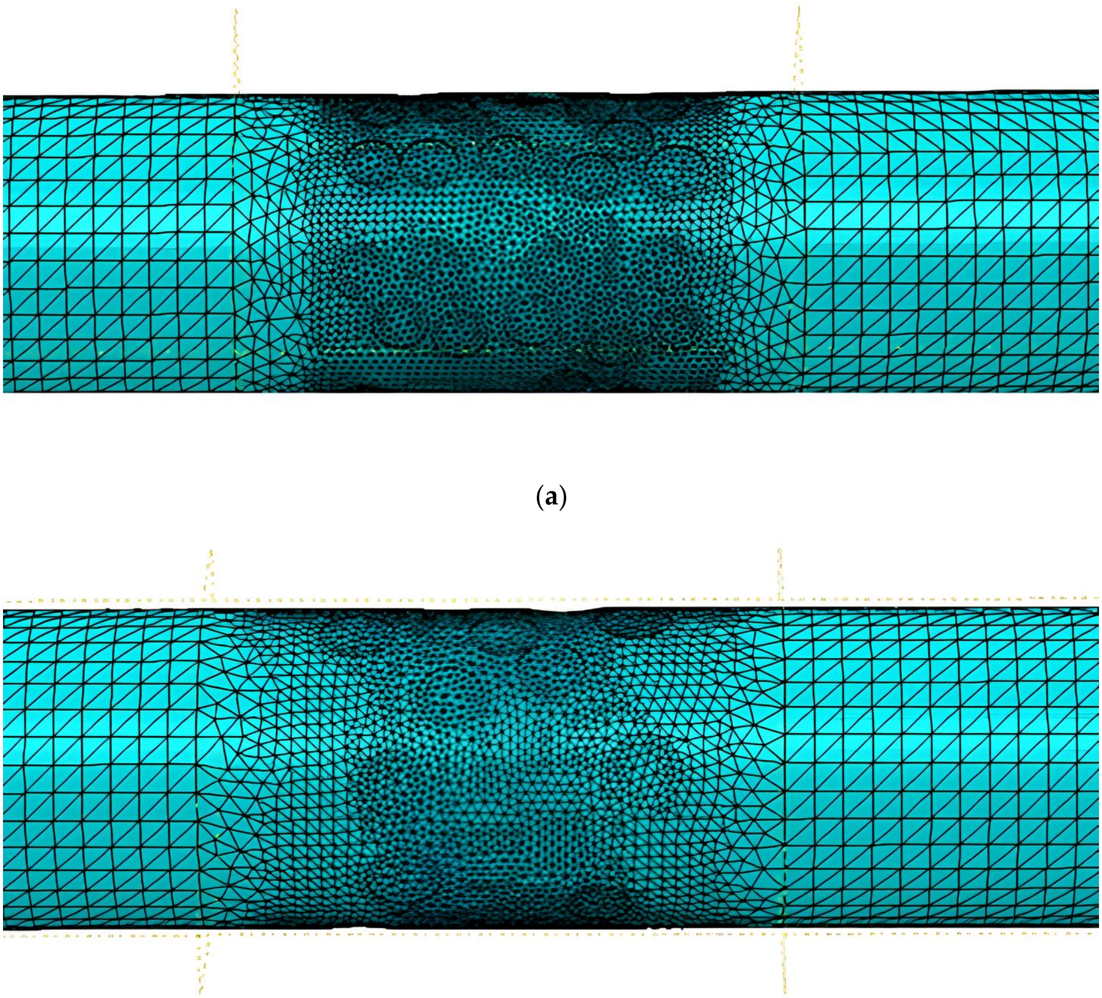
(a)
(b)

Figure 4. Mesh generation of models (**a**) with a large number of pits; (**b**) with a small number of pits.

3. Mechanical Properties

The mechanical properties of the steel column specimens under axial compression suffering local random pitting were investigated, clarifying the variation law of mechanical properties of specimens, which provided evidence for the determination of the critical corrosion rate.

3.1. Experiment and FEM Analysis of Non-Pitting Specimens

The experiment and the finite element analysis of X52Q marine high-strength seamless steel tube were carried out to guarantee the reliability and accuracy of the numerical simulation. Mechanical properties under axial compression were investigated. Table 4 shows the material properties of the specimens. Figure 5 shows the specimen after cutting processing. The electro-hydraulic servo pressure testing machine YAW-5000 was used to apply the axial compression. Constraint conditions were fixed and hinged at both ends of the specimen, which was achieved by a spherical hinge. Figure 6 shows the experimental setup.

Table 4. Material properties of steel.

$E(\mathrm{N/mm^2})$	μ	$\rho(\mathrm{t/mm^3})$	f_{y1}/MPa	f_{u1}/MPa
2.38×10^5	0.3	8.104×10^{-9}	460	555

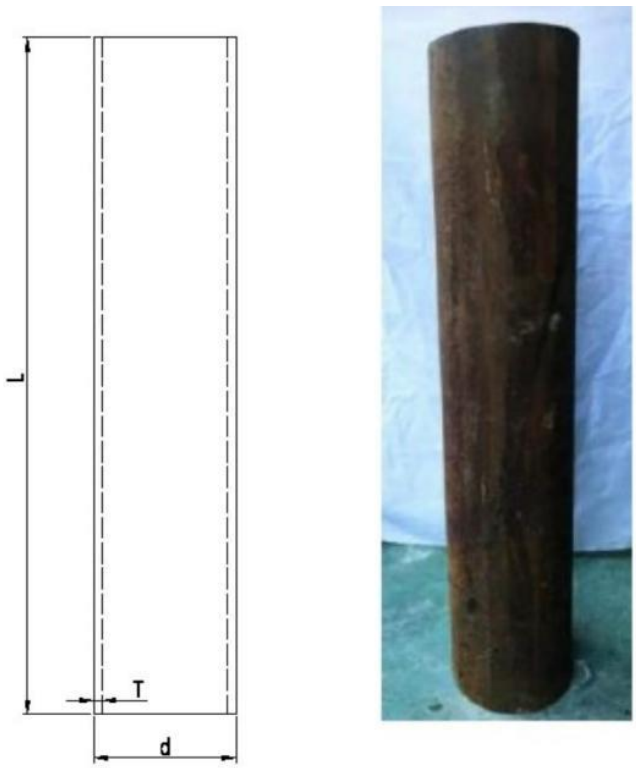

Figure 5. Specimen geometry.

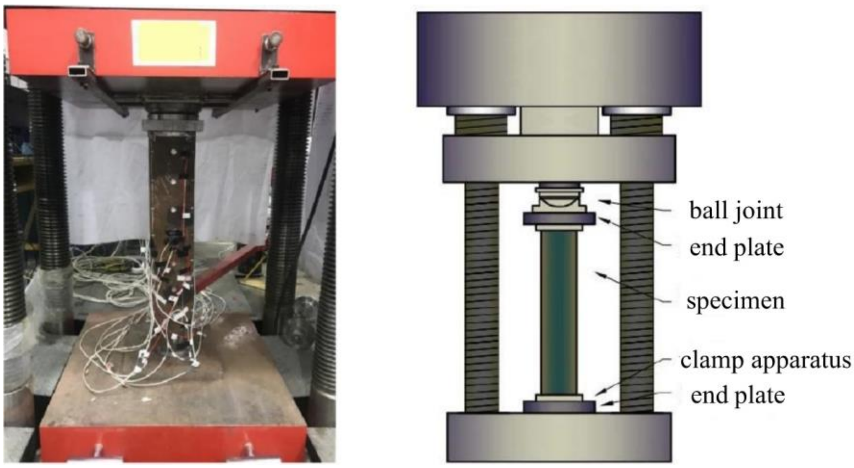

Figure 6. Experimental setup.

ABAQUS was used to conduct FE modeling and analysis of non-pitting specimens. Considering material elastic–plastic and geometric nonlinearity, the real stress was calculated by Equations (13) and (14), where l_0, A_0, l, and A are the initial length, the initial area, the length, and the area after loading of the specimen, respectively. Figure 7 describes the real stress–strain relationship compared with the nominal one. The element type was C3D10. Boundary conditions were set at the bottom surface of the model where the displacement of U1, U2, and U3 was 0. Kinematic coupling was set to connect the concentric point of the top surface, and the displacement of the coupling point in the U1 and U2 directions was 0. The point force was loaded at the coupling point, as shown in Figure 8. Considering the initial imperfection, the displacement of nodes under the first-order buckling mode of the specimen was imported to the subsequent nonlinear buckling analysis model, which is described in Figure 9. To make a full comparison, Qin's study [20] was also cited as a reference.

$$\sigma_{test} = \frac{F}{A_0} \tag{13}$$

$$\sigma_{real} = \frac{F}{A} = \frac{F}{A_0 \frac{l_0}{l}} = \sigma_{test}(1 + \varepsilon_{test}) \tag{14}$$

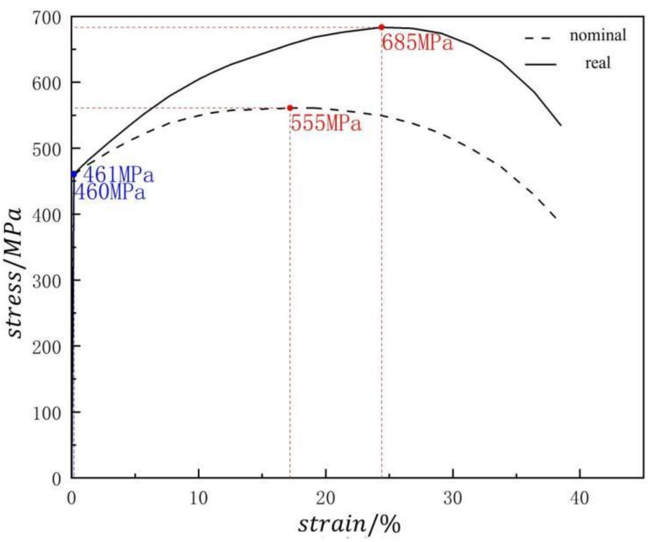

Figure 7. Stress–strain relationship curve.

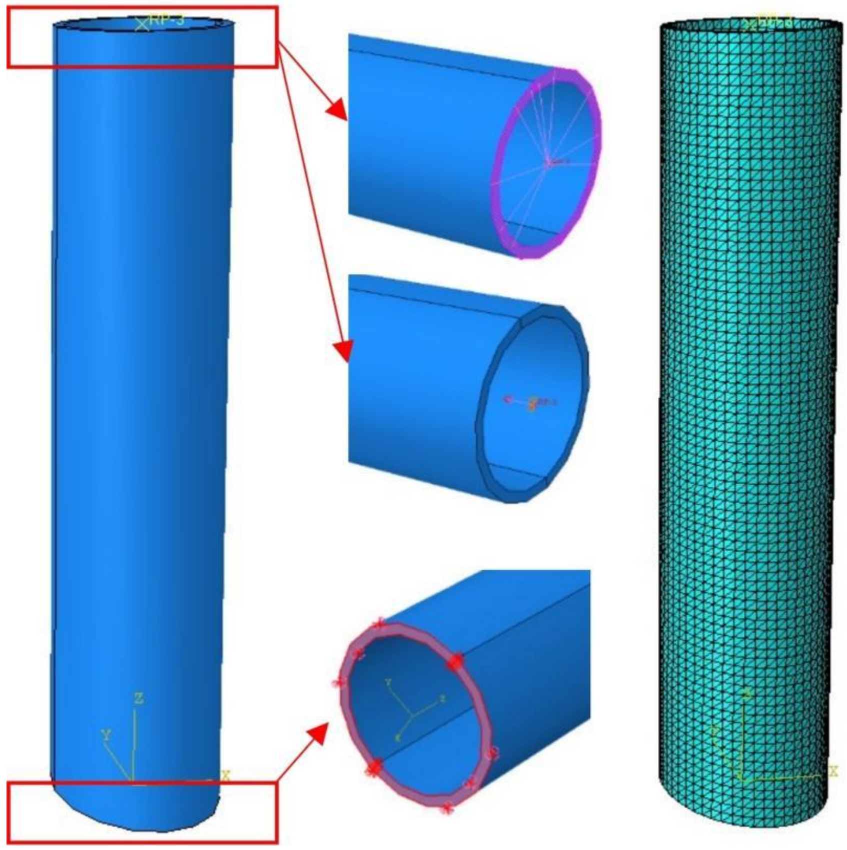

Figure 8. Finite element modeling and boundary conditions.

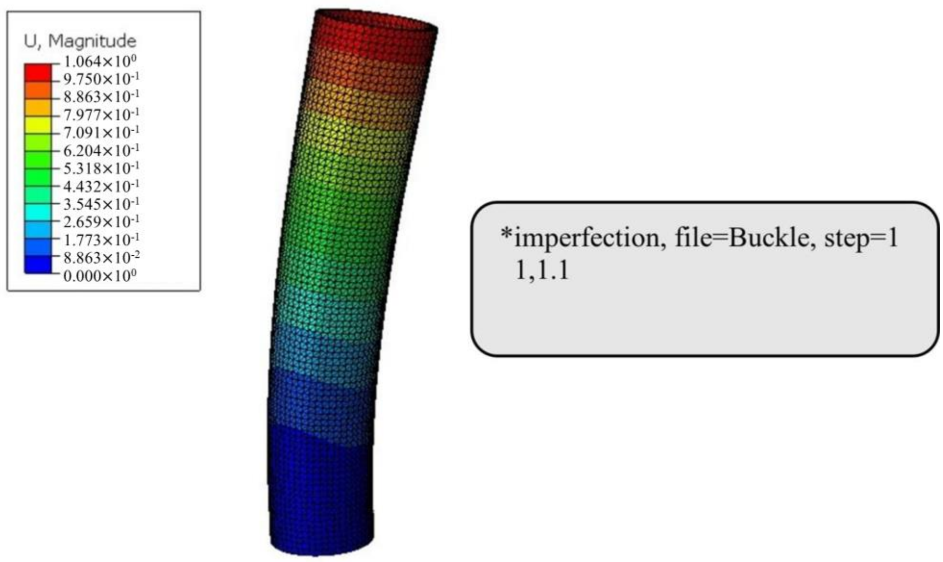

Figure 9. T First-order buckling mode and initial imperfection.

Figure 10 shows the deformation mode of the specimen under the load condition. The deformation pattern was highly consistent with the experiment mode and Qin's result. The ultimate strength is shown in Table 5, and Figure 11 shows the displacement curve. According to the deformation mode, the ultimate strength, and the displacement curve, the FE model showed a high concordance with the experiment, proving that the FE model proposed in this paper was reasonable and accurate. Thus, the following FE analyzing results could be trusted with reasonable accuracy.

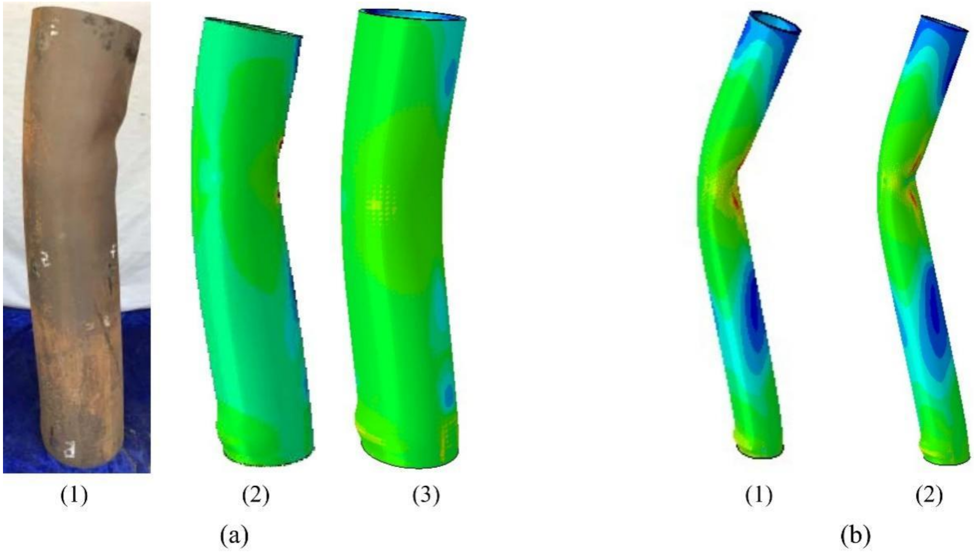

Figure 10. Deformation of the specimen. (**a**) λ = 12.22, (1) Experiment [20], (2) Qin's FEM result [20], and (3) FEM result of this paper; (**b**) λ = 25, (1) Qin's FEM result [20], and (2) FEM result of this paper.

Table 5. The ultimate strength of the specimen.

λ	Experimental Result	Qin's FE Result	FEM Result	Error 1	Error 2
12.22	2424	2384.3	2446.1	0.90%	2.60%
25	-	2315.6	2237.2	-	3.40%

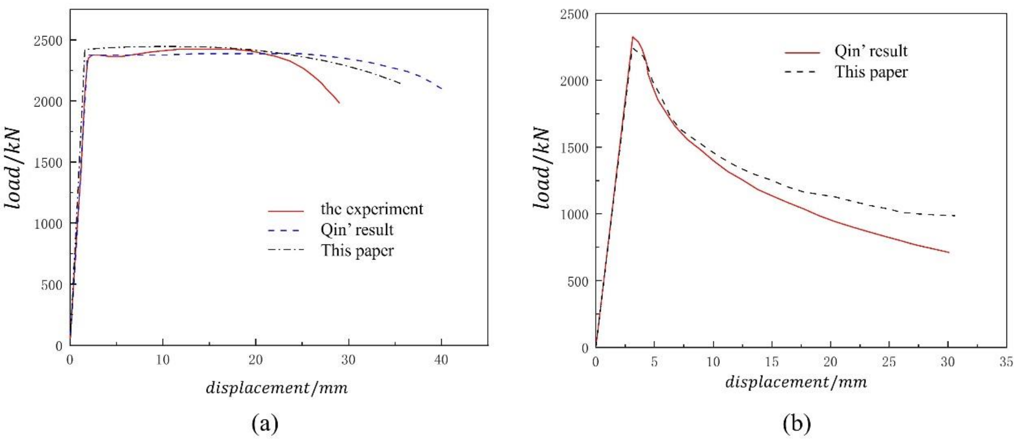

Figure 11. Displacement curve; (**a**) λ = 12.22; (**b**) λ = 25.

3.2. Influence of Local Random Pitting Rate

Using the methods proposed in Section 2, local random pitting models in which λ = 25 were employed, and the ultimate strength F_u of the models was calculated with the method in Section 3.1. Figure 12 shows the deformation modes of the models where local pitting was randomly generated in regions 1~8. Considering the randomness of the size and the location of the pits, the lower limit of ultimate strength in a 95% confidence interval was taken as F_u of the specimens corresponding to each pitting corrosion rate P_0 and corrosion region. Figure 13 shows the regression results of the variation trend of F_u using the least-squares method with variable P_0 in different corrosion regions.

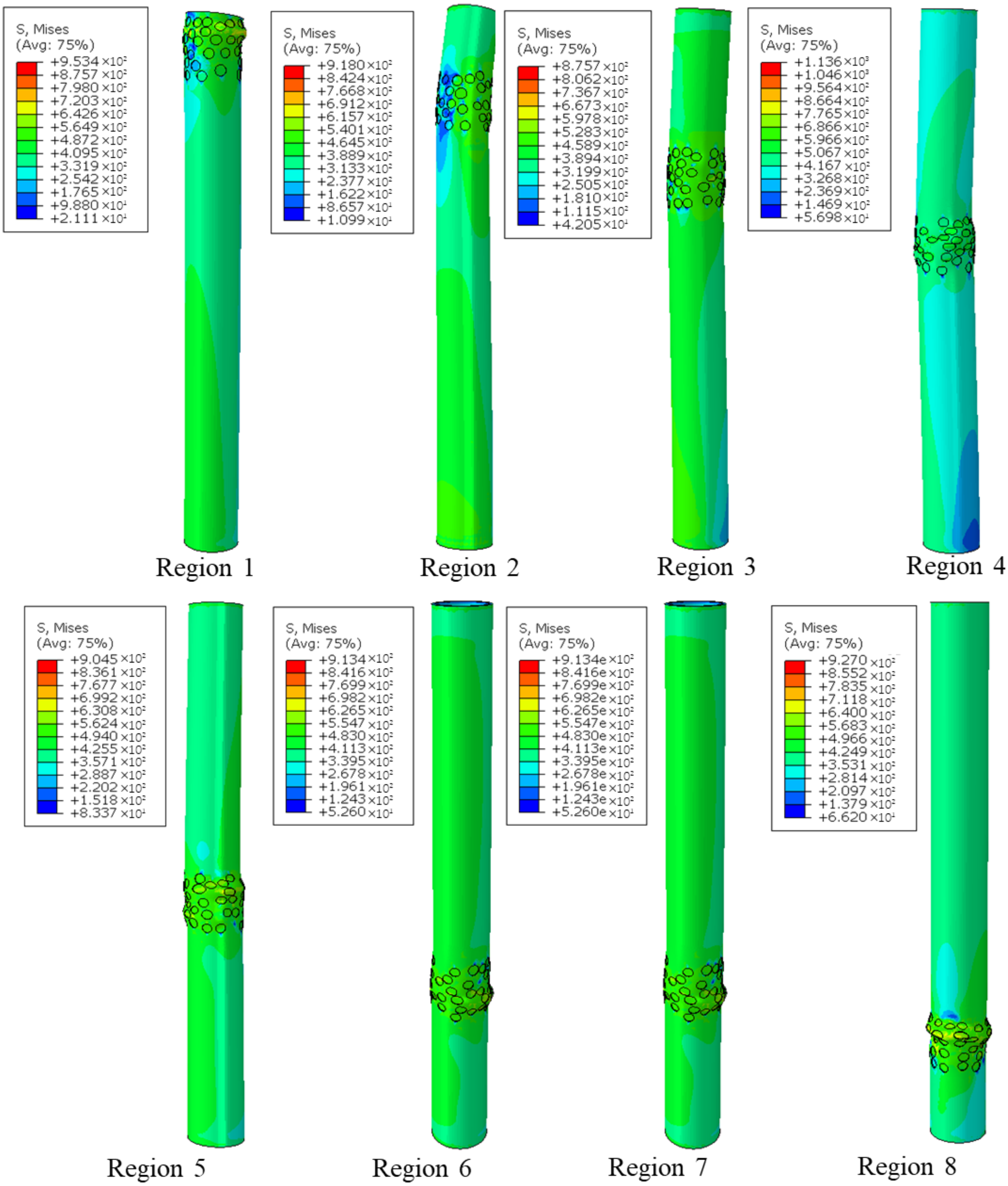

Figure 12. Deformation modes of models.

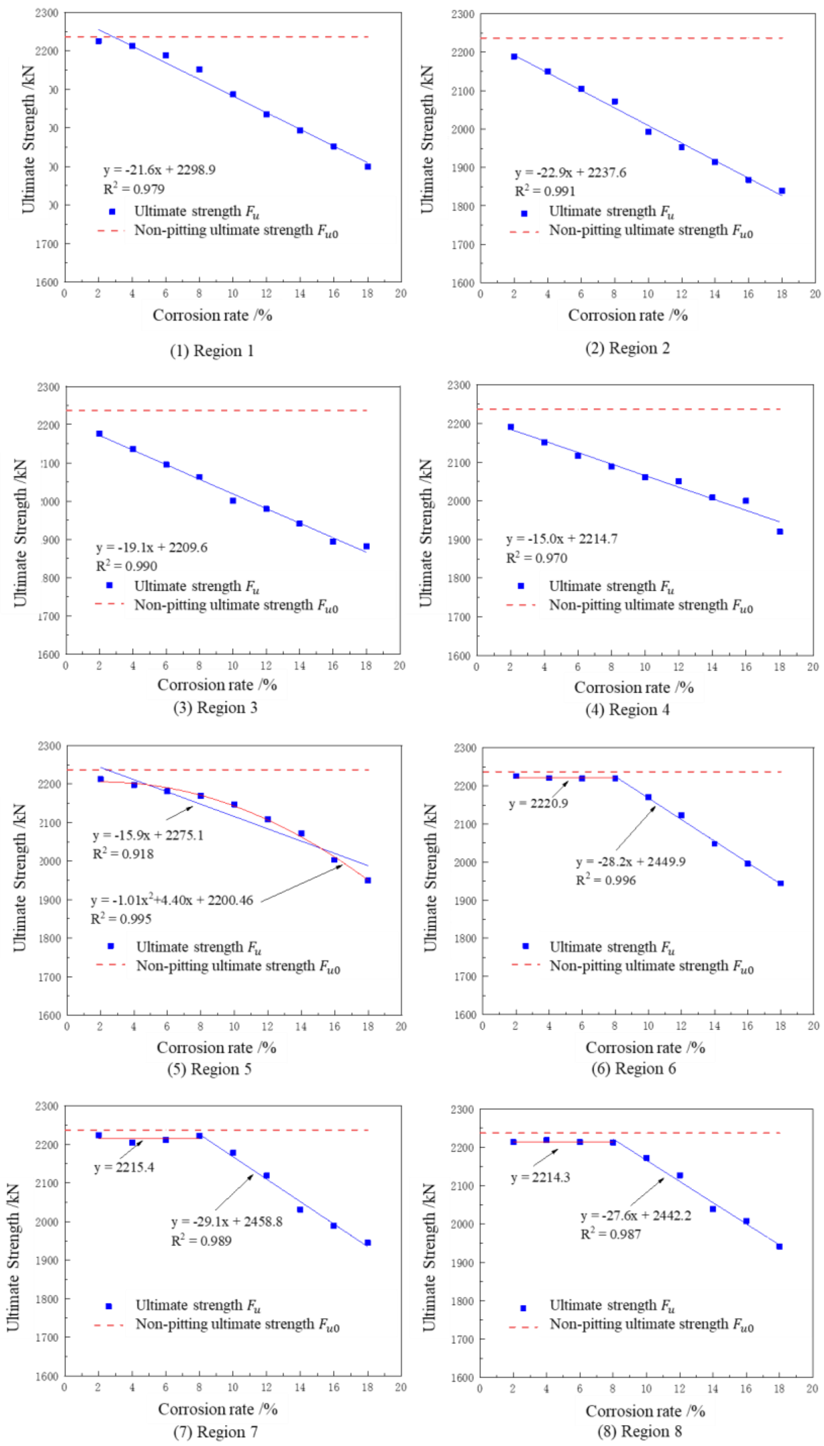

Figure 13. Ultimate strength with variable P_0 in different corrosion regions.

For regions 1~3, F_u decreased linearly with the increase in pitting corrosion rate P_0. The minimum value of R^2 was 0.979, which showed an apparent linear trend. The slope of the fitted results took values in the range [−22.9, −19.1] with a mean value of −21.1, and the intercept took values in the range [2209.6, 2298.9] with a mean value of 2248.7. The variation coefficients γ_s = 9.1% and γ_i = 2.0% indicated a high trend consistency of F_u with P_0 in regions 1~3. The difference between the mean value of the intercept and the F_u of the non-pitting specimen was 0.5%, which showed the rationality of the fitting result. For region 4, F_u decreased linearly with the increase in P_0, with R^2 = 0.970. The difference between the mean value of the intercept and the F_u of non-pitting specimen was 1.0%.

For region 5, F_u showed a secondary parabolic decreasing trend with the increase in P_0, with R^2 = 0.995. For regions 6–8, F_u remained constant when corrosion rate P_0 < 8%, which meant the low R_0 had little effect on P_u when pitting occurred in regions 6~8. F_u decreased linearly with the increase in P_0 when P_0 > 8%, with R^2 > 0.987. The slope of the fitted results took values in the range [−29.1, −27.6] with a mean value of −28.3, and the intercept took value in the range [2442.2, 2458.5] with a mean value of 2450.3. The variation coefficients γ_s = 2.7% and γ_i = 0.3% showed a high trend consistency. This paper holds that the decrease in the ultimate strength of the specimen was caused by the stress concentration and section weakening caused by pitting corrosion. With the increase in pitting corrosion rate, the influence of stress concentration on ultimate strength was less sensitive than that of section weakening.

4. CNN for Pitting Detection

In this section, the critical pitting corrosion rate P_{cr} is defined according to the ultimate strength calculated in Section 3 and related specifications, and the CNN method for the pitting detection of the steel columns is developed based on P_{cr} and the database of vibration modes of the component where the slenderness ratio equals 25.

4.1. Critical Pitting Corrosion Rate

To satisfy the structure's safety and the economy's benefits, the critical strength of non-pitting columns under axial compression F_{cr} was calculated according to GB50017-2017 code [45] using Equation (15), where φ = 0.952 was the stability coefficient of columns, and f_d was the tensile strength of X52Q. F_{cr} was compared with F_u under different P_0 in Figure 13 when P_0 = 12%, the minimum F_u of regions 1~8 was 1951.9 kN, and the minimum F_u = 1992.6 kN when P_0 = 10%. So, the critical pitting rate P_{cr} was defined as 10% to ensure that $F_u > F_{cr}$.

$$F_{cr} = \varphi A_0 f_d = 1960.0kN \tag{15}$$

4.2. Dataset

The dataset of the vibration modes of the specimen was based on the pitting model proposed in Section 2. The specimens were divided into 'corrosion damaged' and 'corrosion undamaged' based on P_{cr}. Reference points, which are the octant points in each pitting model, were set to output the displacement of the first six vibration modes. Figure 14 illustrates the location of the reference points. Two dimensions of vibration, UX and UY, were considered to determine the displacement. When calculating the dataset, pitting FE models were developed based on the specimen in Section 3, which was λ = 25, and committed to ABAQUS to analyze using the subspace iteration method. Python scripts were coded to obtain the first six vibration displacements of the points from the analytical result files.

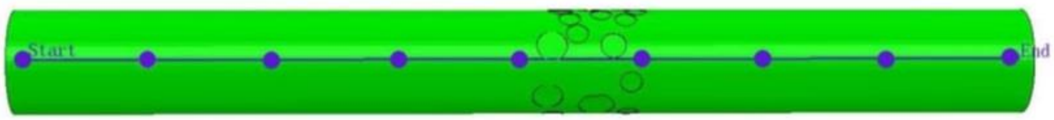

Figure 14. Vibration reference points of specimen.

Figure 15 shows the diagram of the dataset, where U1 and U2 represent the dimension of X and Y, respectively, and the numbers 0 and 1 indicate the judgment of damage to the specimen. The data volume of the dataset was 5376 with the same number of damaged and undamaged specimens. The vibration mode data had a dimension of 9 × 6 after normalization and standardization using the Z-Score method. To ensure this, the vibration features learned by the CNN were not only applicable to the training set but also to the validation set, and the same mean and standard deviation were applied to the training and validation set when conducting the normalization and standardization.

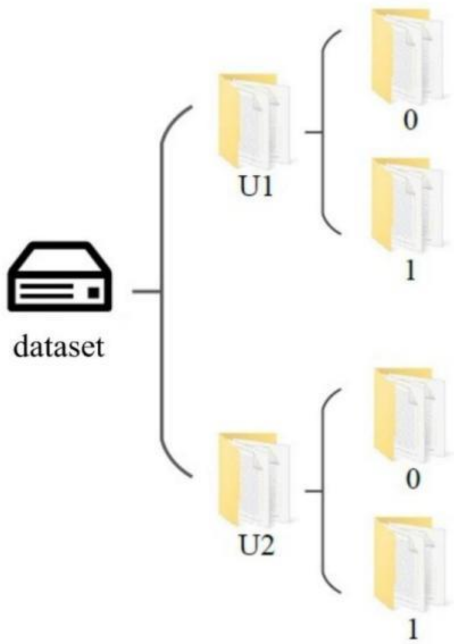

Figure 15. Diagram of dataset.

4.3. CNN

A CNN was developed to determine the corrosion damage to the specimen. Considering that already existing CNNs such as AlexNet have a complex structure and a large number of network layers, which consume a mass of calculation resources, we designed a new CNN. The network consisted of the input and output layers, two convolution layers, two max-pooling layers, and three FC layers. Figure 16 illustrates the structure of the network. The dimension of the input data was $2 \times 9 \times 6$, which means the first six vibration displacements of nine reference points in UX and UY directions were considered. The detailed information on each layer is shown in Table 6. To avoid overfitting, the joint adaptation between the weakened neuron nodes was eliminated to improve the generalization ability of the network, and dropout (P = 0.3) was utilized to abandon parts of the neuron. The index of the max-value of the output layer represented the prediction result of the damaged or undamaged state of the specimen.

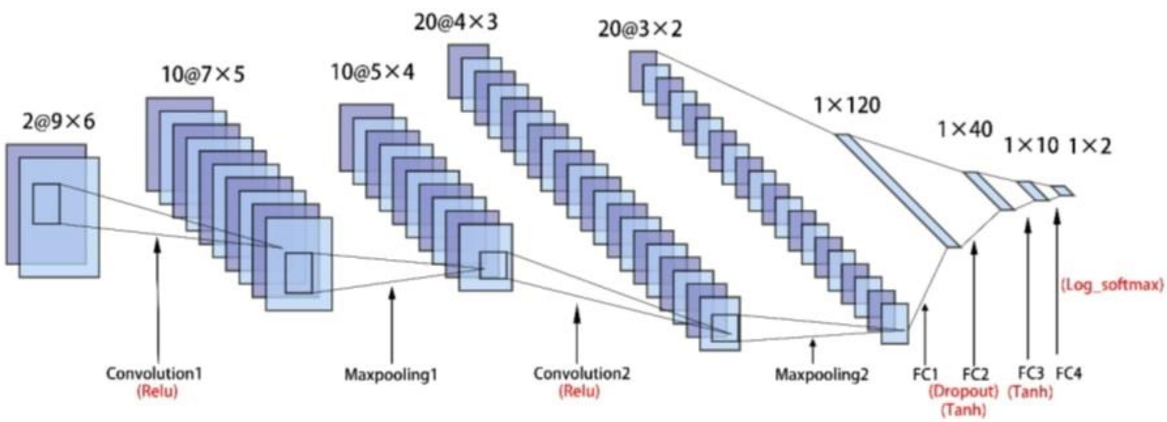

Figure 16. Structure of the CNN.

Table 6. Initial layers in the CNN.

Layer Name	Number of Filters	Size or Dropout Rate	Output Size
Input layer	-	-	2 × 9 × 6
Convolution layer 1	10	3 × 2	10 × 7 × 5
Max-pooling layer 1	-	3 × 2	10 × 5 × 4
Convolution layer 2	20	2 × 2	20 × 4 × 3
Max-pooling layer 2	-	2 × 2	20 × 3 × 2
Fully connected layer 1	-	-	1 × 120
Dropout	-	0.3	-
Fully connected layer 2	-	-	1 × 40
Fully connected layer 3	-	-	1 × 10
Output layer	-	-	1 × 2

The parameters were initialized uniformly in the CNN. The activate function was Relu in convolution1 and convolution2 and Tanh in FC2 and FC3. Log_softmax was the classification function, and Nll_loss was the loss function. MBDG was utilized as the gradient descent method to improve the accuracy. After several attempts, MBDG combined the training speed and convergence accuracy of this CNN when the batch size equaled 21 or 28.

The dataset was divided into a training set and a validation set at a ratio of 50%. The epoch was set as 150, and the batch size was set as 28 with 96 data loaders in each batch. The total number of iterations was 14,400. When a parameter was updated, a momentum that was set as 0.65 improved the accuracy of the network. The initial learning rate was 0.05. An adaptive learning rate function, the scheduler, was defined to adapt the learning rate to half of it when the accuracy was not improved within five training steps.

5. Results and Discussion

Figure 17 illustrates the loss function decrease curve of the training set. The loss began to converge after 10,000 iterations when the adjacent average method was applied. The loss of the training set decreased from 0.73 at the beginning to 0.58 at the end and gradually stabilized, which proved the training was effective. Figure 18a illustrates the loss of the valid set, with the loss decreasing from 0.69 at the beginning to 0.59 at the end. It can be observed that the loss of training and validation both decreased in a lower magnitude. The pitting damage determination accuracy is shown in Figure 18b, which increased from 50% to 75.5% with P_{cr} = 10%. It can be seen that the accuracy was low for the binary classification of damage determination, which did not satisfy the requirements for damage determination, so the network needed to be modified.

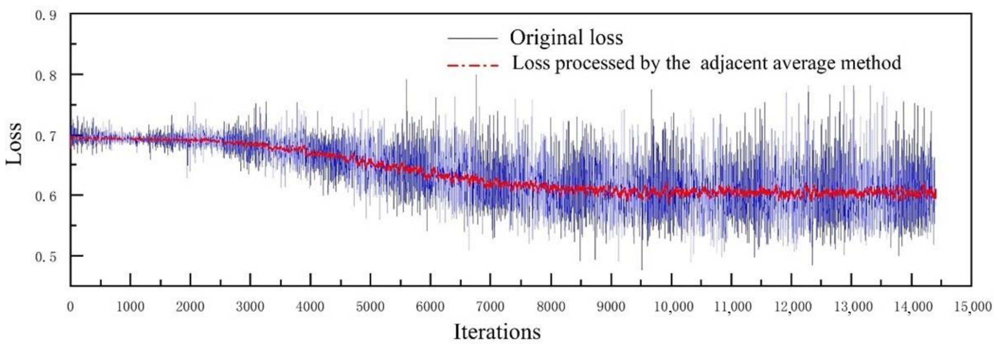

Figure 17. Loss of training set.

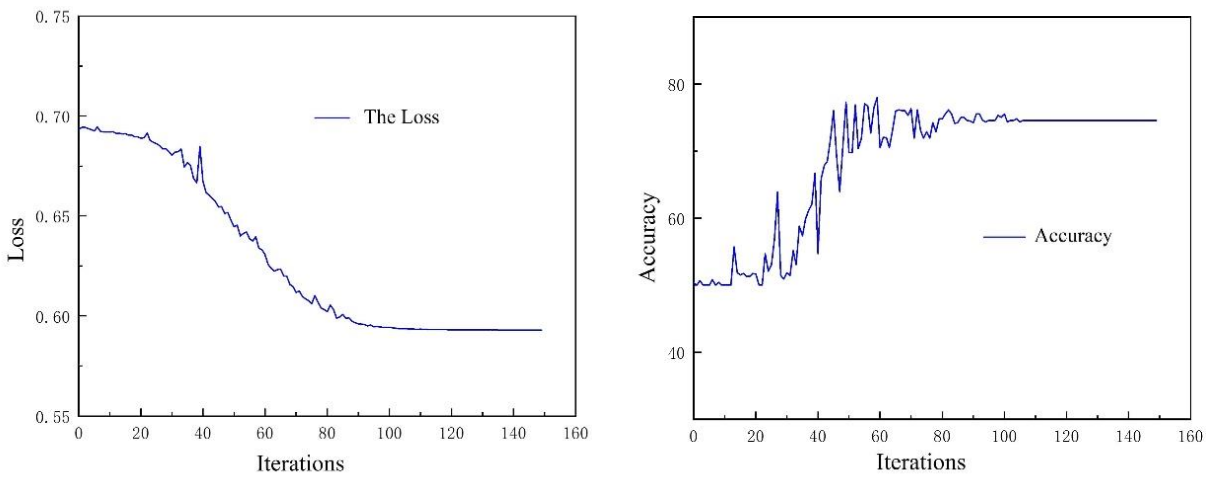

(**a**) (**b**)

Figure 18. (**a**) Loss of validation set; (**b**) accuracy of study.

After many attempts, we found that the accuracy could not be effectively improved by modifying the network structure or parameter settings, so the dataset was adjusted. Considering the random pitting in the four dimensions of depth, size, location, and quantity, the vibration mode difference between specimens with the same pitting region and the adjacent P_0 was relatively small. This led to the fact that even if the CNN had a significant nonlinear fitting ability, it was hard to distinguish the undamaged specimens with P_0 = 10% and the damaged specimens with P_0 = 12%. In practice, it made no difference whether the component with P_0 = 10% was judged as damaged or undamaged. The safety redundancy of pitting protection was increased if the component with P_0 = 10% was determined to be damaged, or the P_{cr} standard was satisfied if it was determined to be undamaged. Thus, the data with P_0 = 10% could be removed from the database to increase the difference between the vibration modes of damaged and undamaged specimens, which improved the training effect of the network.

The data with P_0 = 10% were removed from the database, while an equal number of data with P_0 = 2–8% were added. The new dataset was divided into a training set and a validation set at a ratio of 50%. The iteration epoch was set as 150, and the batch size was set as 21 with 128 data loaders in each batch, with other learning parameters were kept the same. Figure 19 illustrates the loss function decrease curve of the training set. With the modification of the dataset, the loss of the training set decreased from 0.76 at the beginning to 0.20 at the end and gradually stabilized, which had a decreasing amplitude five times larger than the unmodified training set. The change in the loss proved the effectiveness of the training of the network. Figure 20a shows the loss of the validation set, with the loss decreasing from 0.69 at the beginning to 0.26 at the end, which had a decreasing amplitude four times larger than the unmodified validation set. We determined that the adjustment of the dataset can improve the convergence and effectiveness of the network to a higher extent.

Figure 20b shows the correct damage determination curves of the training set with the number of iterations after the modification of the dataset. During the training process, the correct rate of determining damage by using P_{cr} = 10% as the critical corrosion rate gradually increased from 50% to 90.2%, which was 14.7% higher than 75.5% (the vibration samples when P_0 = 10% corrosion rate were not removed). It further demonstrated the accuracy of pitting damage determination by the convolutional neural network, which is of strong practical significance and theoretical value.

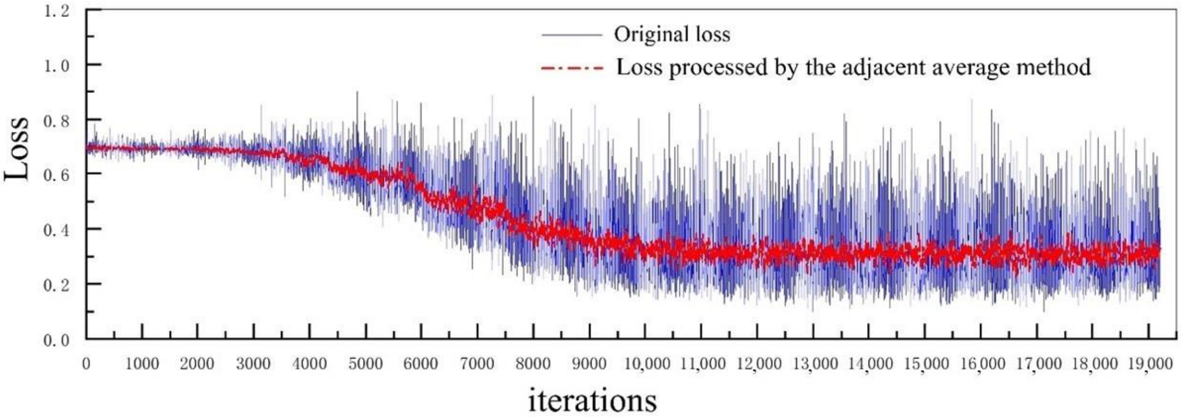

Figure 19. Loss of training set after modification.

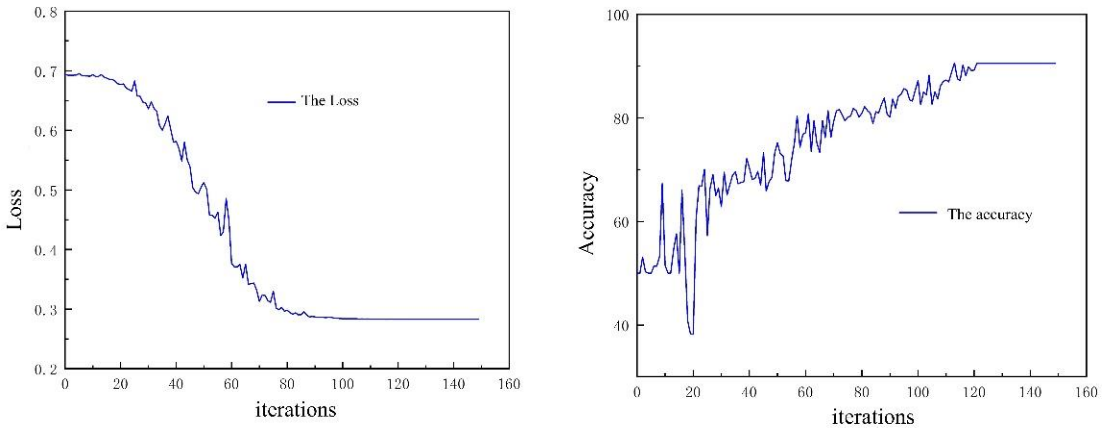

(**a**) (**b**)

Figure 20. (**a**) Loss of validation set after modification; (**b**) accuracy of study.

6. Conclusions

This paper combined numerical simulation and theoretical analysis to carry out systematic research on the ultimate strength of localized random pitting steel components and established localized random pitting damage determination methods using the CNN. In this paper, first, a numerical simulation of random pitting was realized by establishing a multi-parameter localized random pitting numerical model, combined with Python language and ABAQUS finite element software. Then, using cylindrical steel columns for offshore steel platforms as the study object, the mechanical properties of the axial compression under localized random pitting were investigated to clarify the critical corrosion rate to determine the damage. Finally, the critical pitting rate of the cylindrical steel column was determined, and a convolutional neural network was built and trained to determine the damage by inputting the vibration mode of the steel column as the classification criterion, and the accuracy and effectiveness of the neural network were demonstrated. Conclusions can be drawn as follows:

(1) The accuracy of the numerical model. The multi-parameter localized random pitting numerical model established herein can fully express the randomness of pitting pits in shape and location while ensuring the reasonable shape parameters and location coordinates of pitting pits, which can fully describe the realistic pitting situation of steel columns.

(2) Statistical patterns of bearing capacity of localized random pitting corrosion in steel columns. With low dispersion, the ultimate strength distribution of localized random pitting steel columns has good statistical significance. For steel columns with one end

fixed and one end hinged, the ultimate strength decreases linearly with the increase in the pitting corrosion rate when pitting occurs in regions 1–4; the ultimate strength shows a secondary parabolic downward trend as the pitting corrosion rate increases when pitting occurs in region 5; the bearing capacity of the steel column first remains constant and then shows a linear decrease with the increase in corrosion rate when pitting occurs in regions 6–8.

(3) A pitting detection neural network. This study establishes a convolutional neural network to determine whether a steel component is damaged or not by inputting the first six vibration modes. The network has a high detection accuracy, which meets the practical engineering requirements and proves that it is of great theoretical significance and actual application value to determine the damage to a steel component by the convolutional neural network.

(4) The detection system of random pitting corrosion. Based on the numerical model of random pitting, the critical corrosion rate is defined by studying the ultimate strength of pitting components, and then vibration modes are input to train the convolutional neural network for damage determination; thus, a localized random pitting damage determination network with reasonable accuracy is worked out.

Author Contributions: Methodology, X.J. and X.Q.; Software, B.Z.; Validation, B.Z. and H.D.; Investigation, H.Q. and H.D.; Data curation, H.Q. and B.Z.; Writing—original draft, H.Q.; Writing—review & editing, B.Z.; Supervision, X.J.; Project administration, X.J. and X.Q.; Funding acquisition, X.Q. All authors have read and agreed to the published version of the manuscript.

Funding: The financial support of the National Natural Science Foundation of China (52278206 and 52278207), the National Key R&D Program of China (2020YFD1100403), Natural Science Foundation of Shanghai (21ZR1466100), and Fundamental Research Funds for the Central Universities (02002150114) are highly appreciated.

Institutional Review Board Statement: Not applicable.

Informed Consent Statement: Not applicable.

Data Availability Statement: Not available due to privacy or ethical restrictions.

Conflicts of Interest: The authors declare no conflict of interest.

References

1. Frankel, G.S. Pitting corrosion of metals—A review of the critical factors. *J. Electrochem. Soc.* **1998**, *145*, 2186–2198. [CrossRef]
2. Peyre, P.; Scherpereel, X.; Berthe, L.; Carboni, C.; Fabbro, R.; Beranger, G.; Lemaitre, C. Surface modifications induced in 316L steel by laser peening and shot-peening. Influence on pitting corrosion resistance. *Mater. Sci. Eng. A-Struct. Mater. Prop. Microstruct. Process.* **2000**, *280*, 294–302. [CrossRef]
3. Guedes Soares, C.; Garbatov, Y.; Zayed, A. Effect of environmental factors on steel plate corrosion under marine immersion conditions. *Corros. Eng. Sci. Technol.* **2011**, *46*, 524–541. [CrossRef]
4. Velázquez, J.; van der Weide, H.; Hernandez-sÁNchez, E.; Hernández, H. Statistical Modelling of Pitting Corrosion: Extrapolation of the Maximum Pit Depth-Growth. *Int. J. Electrochem. Sci.* **2014**, *9*, 4129–4143. [CrossRef]
5. Bhandari, J.; Khan, F.; Abbassi, R.; Garaniya, V.; Ojeda, R. Modelling of pitting corrosion in marine and offshore steel structures—A technical review. *J. Loss Prev. Process Ind.* **2015**, *37*, 39–62. [CrossRef]
6. Pardo, A.; Merino, M.C.; Coy, A.E.; Viejo, F.; Arrabal, R.; Matykina, E. Pitting corrosion behaviour of austenitic stainless steels—Combining effects of Mn and Mo additions. *Corros. Sci.* **2008**, *50*, 1796–1806. [CrossRef]
7. Shi, Y.; Yang, B.; Liaw, P.K. Corrosion-Resistant High-Entropy Alloys: A Review. *Metals* **2017**, *7*, 43. [CrossRef]
8. Qiang, X.; Shen, Y.; Jiang, X.; Bijlaard, F.S.K. Theoretical study on initial stiffness of thin-walled steel T-stubs taking account of prying force. *Thin-Walled Struct.* **2020**, *155*, 106944. [CrossRef]
9. Qiang, X.; Shu, Y.; Jiang, X. Experimental and numerical study on high-strength steel flange-welded web-bolted connections under fire conditions. *J. Constr. Steel. Res.* **2022**, *192*, 107255. [CrossRef]
10. Qiang, X.; Wu, Y.; Wang, Y.; Jiang, X. Novel crack repair method of steel bridge diaphragm employing Fe-SMA. *Eng. Struct.* **2023**, *292*, 116548. [CrossRef]
11. Jiang, X.; Guedes Soares, C. Ultimate capacity of rectangular plates with partial depth pits under uniaxial loads. *Mar. Struct.* **2012**, *26*, 27–41. [CrossRef]

12. Jiang, X.; Guedes Soares, C. A closed form formula to predict the ultimate capacity of pitted mild steel plate under biaxial compression. *Thin-Walled Struct.* **2012**, *59*, 27–34. [CrossRef]
13. Nakai, T.; Matsushita, H.; Yamamoto, N.; Arai, H. Effect of pitting corrosion on local strength of hold frames of bulk carriers (1st report). *Mar. Struct.* **2004**, *17*, 403–432. [CrossRef]
14. Pidaparti, R.M.; Palakal, P.J.; Fang, L. Cellular automation approach to model aircraft corrosion pit damage growth. *Aiaa J.* **2004**, *42*, 2562–2569. [CrossRef]
15. Miao, C.Q.; Yu, J.; Mei, M.X. Distribution law of corrosion pits on steel suspension wires for a tied arch bridge. *Anti-Corros. Methods Mater.* **2016**, *63*, 166–170. [CrossRef]
16. Sharifi, Y. Reliability of deteriorating steel box-girder bridges under pitting corrosion. *Adv. Steel Constr.* **2011**, *7*, 220–238.
17. Zhang, X.Z.; Liu, R.; Chen, K.Y.; Yao, M.X. Pitting Corrosion Characterization of Wrought Stellite Alloys in Green Death Solution with Immersion Test and Extreme Value Analysis Model. *J. Mater. Eng. Perform.* **2014**, *23*, 1718–1725. [CrossRef]
18. Ossai, C.I.; Boswell, B.; Davies, I. Markov chain modelling for time evolution of internal pitting corrosion distribution of oil and gas pipelines. *Eng. Fail. Anal.* **2016**, *60*, 209–228. [CrossRef]
19. Rivas, D.; Caleyo, F.; Valor, A.; Hallen, J.M. Extreme value analysis applied to pitting corrosion experiments in low carbon steel: Comparison of block maxima and peak over threshold approaches. *Corros. Sci.* **2008**, *50*, 3193–3204. [CrossRef]
20. Melchers, R.E. Pitting corrosion of mild steel in marine immersion environment-Part 2: Variability of maximum pit depth. *Corrosion* **2004**, *60*, 937–944. [CrossRef]
21. Wang, Y.; Wharton, J.A.; Shenoi, R.A. Ultimate strength analysis of aged steel-plated structures exposed to marine corrosion damage: A review. *Corros. Sci.* **2014**, *86*, 42–60. [CrossRef]
22. Sultana, S.; Wang, Y.; Sobey, A.J.; Wharton, J.A.; Shenoi, R.A. Influence of corrosion on the ultimate compressive strength of steel plates and stiffened panels. *Thin-Walled Struct.* **2015**, *96*, 95–104. [CrossRef]
23. Cawley, P.; Adams, R.D. The location of defects in structures from measurements of natural frequencies. *J. Strain Anal. Eng. Des.* **1979**, *14*, 49–57. [CrossRef]
24. Salawu, O.S. Detection of structural damage through changes in frequency: A review. *Eng. Struct.* **1997**, *19*, 718–723. [CrossRef]
25. Xiao, F.; Meng, X.; Zhu, W.; Chen, G.; Yan, Y. Combined Joint and Member Damage Identification of Semi-Rigid Frames with Slender Beams Considering Shear Deformation. *Buildings* **2023**, *13*, 1631. [CrossRef]
26. Xiao, F.; Zhu, W.; Meng, X.; Chen, G. Parameter Identification of Structures with Different Connections Using Static Responses. *Appl. Sci.* **2022**, *12*, 5896. [CrossRef]
27. Pandey, A.K.; Biswas, M.; Samman, M.M. Damage detection from changes in curvature mode shapes. *J. Sound Vib.* **1991**, *145*, 321–332. [CrossRef]
28. Wang, S.; Li, H.-J. Assessment of structural damage using natural frequency changes. *Acta Mech. Sin.* **2012**, *28*, 118–127. [CrossRef]
29. Zhang, X.W.; Zhao, S.L.; Wang, Z.; Li, J.X.; Qiao, L.J. The pitting to uniform corrosion evolution process promoted by large inclusions in mooring chain steels. *Mater. Charact.* **2021**, *181*, 12. [CrossRef]
30. Xiao, F.; Sun, H.; Mao, Y.; Chen, G. Damage Identification of Large-Scale Space Truss Structures Based on Stiffness Separation Method. *Structures* **2023**, *53*, 109–118. [CrossRef]
31. Ben Seghier, M.E.; Keshtegar, B.; Taleb-Berrouane, M.; Abbassi, R.; Trung, N.T. Advanced intelligence frameworks for predicting maximum pitting corrosion depth in oil and gas pipelines. *Process Saf. Environ. Protect.* **2021**, *147*, 818–833. [CrossRef]
32. Ossai, C.I. A Data-Driven Machine Learning Approach for Corrosion Risk Assessment—A Comparative Study. *Big Data Cogn. Comput.* **2019**, *3*, 28. [CrossRef]
33. Sasidhar, K.N.; Siboni, N.H.; Mianroodi, J.R.; Rohwerder, M.; Neugebauer, J.; Raabe, D. Deep learning framework for uncovering compositional and environmental contributions to pitting resistance in passivating alloys. *NPJ Mater. Degrad.* **2022**, *6*, 10. [CrossRef]
34. Sharifi, Y.; Tohidi, S. Ultimate capacity assessment of web plate beams with pitting corrosion subjected to patch loading by artificial neural networks. *Adv. Steel Constr.* **2014**, *10*, 325–350.
35. Ossai, C.I. Corrosion defect modelling of aged pipelines with a feed-forward multi-layer neural network for leak and burst failure estimation. *Eng. Fail. Anal.* **2020**, *110*, 15. [CrossRef]
36. Barai, S.V.; Pandey, P.C. Vibration Signature Analysis Using Artificial Neural Networks. *J. Comput. Civ. Eng.* **1995**, *9*, 259–265. [CrossRef]
37. Qiao, Y.X.; Xu, D.K.; Wang, S.; Ma, Y.J.; Chen, J.; Wang, Y.X.; Zhou, H.L. Effect of hydrogen charging on microstructural evolution and corrosion behavior of Ti-4Al-2V-1Mo-1Fe alloy. *J. Mater. Sci. Technol.* **2021**, *60*, 168–176. [CrossRef]
38. Cha, Y.J.; Choi, W.; Suh, G.; Mahmoudkhani, S.; Buyukozturk, O. Autonomous Structural Visual Inspection Using Region-Based Deep Learning for Detecting Multiple Damage Types. *Comput.-Aided Civ. Infrastruct. Eng.* **2018**, *33*, 731–747. [CrossRef]
39. Chun, P.; Yamane, T.; Izumi, S.; Kameda, T. Evaluation of Tensile Performance of Steel Members by Analysis of Corroded Steel Surface Using Deep Learning. *Metals* **2019**, *9*, 1259. [CrossRef]
40. Gupta, R.D.; Kundu, D. Generalized exponential distributions. *Aust. N. Z. J. Stat.* **1999**, *41*, 173–188. [CrossRef]
41. Wallace, J.; Reddy, R.; Pugh, D.; Pacheco, J. Sour Service Pit Growth Predictions of Carbon Steel using Extreme Value Statistics. In Proceedings of the CORROSION 2007, Nashville, TN, USA, 11–15 March 2007.
42. Keliang, R.E.N.; Guozhi, L.U.; Yohong, Z. Stochastic Arrange and Computer Simulation of Corrosion Pitting in Damage Structure. *Acta Aeronaut. Et Astronaut. Sin.* **2006**, *27*, 459–462.

43. Wang, Y.W.; Wu, X.Y.; Zhang, Y.H.; Huang, X.P.; Cui, W. Pitting corrosion model of mild and low-alloy steel in marine environment-Part 2: The shape of corrosion pits. *J. Ship Mech.* **2007**, *11*, 735–743.
44. Qin, J.Y. Study on Mechanical Properties of Marine Steel Pipe considering Pitting Damage. Master's Thesis, Dalian University of Technology, Dalian, China, 2020.
45. *GB50017-2017*; Standard for Design of Steel Structures. Ministry of Housing and Urban-Rural Development: Beijing, China, 2017.